Observation of non-dormant persister cells reveals diverse modes of survival in antibiotic persistence

Miki Umetani,[1,2,3‡] Miho Fujisawa,[3‡] Reiko Okura,[3] Takashi Nozoe,[1,2,3] Shoichi Suenaga,[4] Hidenori Nakaoka,[5] Edo Kussell,[6,7] Yuichi Wakamoto[1,2,3*]

[1]Research Center for Complex System Biology, The University of Tokyo,
[2]Universal Biology Institute, The University of Tokyo
[3]Department of Basic Science, Graduate School of Arts and Sciences, The University of Tokyo
[4]Department of Neuropathology, Graduate School of Medicine, The University of Tokyo
[5]Laboratory of Cell Cycle Regulation, Graduate School of Biostudies, Kyoto University
[6]Department of Biology, New York University
[7]Department of Physics, New York University

‡These authors contributed equally to this study
*To whom correspondence should be addressed; E-mail: cwaka@mail.ecc.u-tokyo.ac.jp.

Abstract

Bacterial persistence is a phenomenon in which a small fraction of isogenic bacterial cells survives a lethal dose of antibiotics. It is generally assumed that persistence is caused by cells with inactive growth generated prior to drug exposure. However, evidence from direct observation is scarce due to the extremely low frequencies of persisters. Here, we visualize the responses of more than 10^6 individual cells of wildtype *Escherichia coli* to lethal doses of antibiotics, sampling cells from different growth phases and culture media. We show that preexisting growth-arrested dormant persisters constitute only minor fractions of persistent cell lineages in populations sampled from exponential phase. Non-dormant persisters survive with radical morphological changes in response to drug exposure, including L-form-like morphologies or filamentation. Incubating cells under stationary phase conditions increases both the frequency and the probability of survival of dormant cells. While dormant cells in late stationary phase express a general stress response regulator, RpoS, at high levels, persistent cell lineages show lower levels of RpoS among the dormant cells. These results demonstrate that diverse survival pathways coexist within bacterial populations to achieve persistence and that persistence does not necessarily require dormant cells.

Introduction

Antibiotics are potent chemotherapeutic substances that are heavily relied upon to counter bacterial infectious diseases. Nonetheless, bacterial cells often circumvent elimination and continue to survive under antibiotics exposure by acquiring genetic changes to enhance their resistance or tolerance, or by producing less susceptible phenotypic variants. Bacterial persistence is a phenomenon in which a small subset of cells in an isogenic cell population survives for a prolonged period under exposure to lethal doses of antibiotics [1–8]. The phenomenon occurs across a wide range of combinations of bacterial species and antibiotics, including clinically important pathogens [8], such as *Mycobacterium tuberculosis* [2, 9, 10], *Staphylococcus aureus* [11, 12], and *Pseudomonas aeruginosa* [13], and consequently, it has been recognized as a global health concern [1–4, 8, 9].

Since the first elaboration of persistence [14], growth-arrested dormant cells generated before drug exposure have been thought to be responsible for the persistence of cellular populations [1–8]. This explanation of persistence was based on the observations that most antibiotics were ineffective to bacterial cell populations under growth-inhibiting conditions, such as low temperature, low nutrients, and presence of bacteriostatic substances [14]. Persistence caused by such prior exposure to stressful environments is now called *triggered persistence* [15]. However, examining this hypothesis by directly observing individual cell lineages is challenging due to extremely low frequencies of surviving cells (typically 10^{-6}-10^{-3} [16]). Consequently, the observation is limited to high persistence mutants [17, 18], to naturally high-persisting combinations of bacterial species and drugs [19, 20], or to conditions that significantly increase the frequencies of surviving cells [21–23]. It therefore remains elusive whether any cellular traits other than dormancy could cause bacterial persistence. In fact, several studies have suggested that persistence occurs without dormant cells [19, 20, 24]. For example, Wakamoto *et*

al. conducted single-cell observation of persistence of *Mycobacterium smegmatis* against isoniazid (INH), revealing that the surviving cells grew normally before drug exposure [19]. Using a cell-sorting assay Orman and Brymildsen showed that even the fast-growing fraction of an exponentially growing *E. coli* population produced cells that survived lethal doses of Amp and ofloxacin [24]. Furthermore, Goormaghtigh and Van Melderen showed by single-cell observation that *E. coli* persisters against ofloxacin in exponential cultures were dividing normally before exposure [20]. These results imply that bacterial persistence occurs even without dormant cells. However, the survival of non-dormant cells is often deemed an exception in bacterial persistence [25]. Furthermore, the diversity of their growth and survival behaviors within a cellular population has not previously been investigated.

To investigate whether dormant cells are indeed predominantly responsible for bacterial persistence, we visualized the response of more than 10^6 individual cells to antibiotics exposure utilizing a microfluidic device and analyzed the persistence of wildtype *E. coli* (MG1655 strain), one of the best-studied model systems of bacterial persistence. Contrary to the prevailing view in the field, we reveal that most surviving cells were actively growing before drug exposure when cell populations sampled from exponential phase were exposed to the β-lactam ampicillin (Amp) or the fluoroquinolone ciprofloxacin (CPFX). By tracking persister lineages before and after antibiotic exposures, we reveal diverse survival pathways that underlie antibiotic persistence.

Results

The MCMA device reveals persistent single-cell lineages

We constructed an *E. coli* strain MF1 that expresses RpoS-mCherry from the native *rpoS* locus on the chromosome. RpoS is a specialized sigma factor controlling the general stress response [26], and its high expression has been suggested to predict persistence [6]. This *E. coli*

strain also expresses green fluorescent protein (GFP) from a low copy plasmid [27] to facilitate visualizing individual cells. The minimum inhibitory concentration (MIC) of MF1 against Amp was 16 μg/mL, which was the same as that of its non-fluorescent parental strain MG1655 (Fig. S1A).

The population killing curve of MF1 sampled from exponential phase exhibited biphasic or multi-phasic decay in LB medium containing 200 μg/ml of Amp (12.5×MIC, Fig. 1A; see Fig. S2A for the growth curve of this strain). Therefore, this *E. coli* strain exhibits persistence in this condition [15]. The decay rate markedly decreased under the Amp exposure from 0.18±0.02 h^{-1} to 0.005±0.003 h^{-1} (Fig. 1A). The frequency of persister cells evaluated at 3 h after the onset of Amp exposure was 4.2×10^{-6} (2.0×10^{-6}-8.8×10^{-6}) (Fig. 1A).

To visualize low-frequency persistent single-cell lineages, we used a microfluidic device equipped with a membrane-covered microchamber array (MCMA; Fig. 1B, 1C, and S3). *E. coli* cells were enclosed in the 0.8-μm deep microchambers etched on a glass coverslip by covering microchambers with a cellulose membrane (Fig. 1C). *E. coli* cells grow in a monolayer and form two-dimensional microcolonies in the microchambers (Fig. 1C, 1D and S3). We can control medium conditions around cells flexibly by the medium flow above the membrane (Fig. 1C and S3). Here, we used the method of attaching cellulose membranes to glass coverslips via biotin-streptavidin binding, which was developed previously and utilized for analyzing bacterial growth and starvation [28–30].

We conducted time-lapse single-cell observation of MF1 cells using the MCMA device, sampling cells from exponential phase. We monitored 110-170 microchambers with a 100× objective in each time-lapse experiment to observe individual cells with a high spatial resolution. After initial pre-culturing periods of 1.5 h without Amp, we exposed cell populations to 200 μg/mL of Amp for 3.5 h. The Amp exposure lysed most cells (Fig. 1D-I, Supplementary Video 1, and Supplementary Video 2). However, we detected two single-cell lineages that sur-

vived and regrew after the Amp exposure in the ten repeated experiments conducted with the MCMA device (Fig. 1D-I, Supplementary Video 1, and Supplementary Video 2). Interestingly, cells grew and divided actively before the Amp exposure in one of the persistent cell lineages (Fig. 1D-F and Supplementary Video 1). In response to the Amp exposure, the cell in this lineage radically changed its cell morphology from a rod shape to a round shape with membrane blebbing and transitted to an L-form-like cell [31] (Fig. 1E and Supplementary Video 1). After drug removal, many progeny of the surviving cell gradually restored rod shapes through multiple cell divisions (Fig. 1D, 1E, and Supplementary Video 1).

The other surviving cell lineage exhibited no growth and division before and during the Amp exposure and restarted growth after drug removal (Fig. 1G-I and Supplementary Video 2). This sequence of growth behavior is consistent with the expected survival dynamics for persistence caused by dormant cells [17]. Hereafter, we refer to the surviving cells that exhibited no growth and division before drug exposure (Fig. 1I) as *dormant persisters* and those that showed growth and division (Fig. 1F) as *non-dormant persisters*.

The expression levels of RpoS-mCherry were low in all the observed cells, including the dormant persister cell characterized above (Fig. 1D, 1G, Supplementary Video 1, and Supplementary Video 2). The suppression of RpoS expression in exponential phases in LB media is consistent with the literature [26, 32].

Persisters are predominantly non-dormant in exponential-phase cell cultures exposed to Amp

To further scale up single-cell observation, we next used a 40× objective and acquired only bright-field images in the time-lapse measurements (Supplementary Video 3). These changes in the microscopy configuration reduced the spatial resolution of acquired images and did not involve acquisition of fluorescence images. However, most single-cell lineages could still be

tracked, and the drug response of more than 10^5 individual cells was observable with a time-lapse interval of 3 min.

We again observed the response of the MF1 cells sampled from exponential phase exposed to 200 μg/mL Amp for 3.5 h, detecting 12 persistent cell lineages (defined as drug-exposed cells that survived Amp exposure and regrew after drug removal) among 3.0×10^5 drug-exposed cells (Supplementary Video 4-6). We found that 10 out of 12 persistent cell lineages were non-dormant cells that grew and divided actively before the Amp exposure (Fig. 2A).

It was reported that persisters of *E. coli hipQ* mutant were non-dormant and grew at suppressed rates in LB medium (0.2∼0.3 doublings/h) [17]. We therefore quantified the pre-exposure growth rates of the observed cell lineages, finding 2.0±0.2 doublings/h for non-dormant persistent cell lineages and 2.32±0.04 doublings/h for non-surviving cell lineages. This result shows that, although their pre-exposure growth rates might be slightly lower than those of non-surviving lineages, non-dormant persisters in wildtype *E. coli* grow significantly faster than *hipQ* persisters.

The dormant persisters that constituted a minor fraction of the persistent cell lineages might come from long-lagging bacteria carried over from the previous stationary phase [23, 33]. To test whether the dormant persister fraction disappears by effectively eliminating long-lagging cells, we prepared the exponential phase cell cultures grown from a 1000-fold more diluted pre-culture cell suspension and repeated the time-lapse measurements (see Methods for detail). We thereby found that dormant persisters still emerged at a comparable frequency: We detected 23 persistent cell lineages among 9.9×10^5 observed cells, and 4 out of 23 persistent cell lineages were dormant persisters (Fig 2A and Supplementary Video 7). This result shows that dormant persisters are observed even without the carry-over of lagging cells and are therefore generated spontaneously in exponential phases without apparent external triggers [15].

Non-dormant persisters are dominant even in minimal medium

To test whether medium conditions influence persistence dynamics, as previously suggested [34], we repeated the experiments with M9 minimal medium. The killing curve of the *E. coli* MF1 cell populations sampled from exponential phase cultures in M9 minimal medium shows a biphasic curve, confirming the occurrence of persistence in this condition (Fig. S4; see Fig. S2B for the growth curve) and indicating a frequency of persister cells that was 4-fold higher than in LB (Fig. S4).

Single-cell time-lapse measurements detected 24 persistent cell lineages that regrew and divided after the exposure to 200 μg/mL of Amp for 6 h among 1.1×10^6 drug-exposed cells. Among them, we were able to determine the presence or absence of growth and division of 19 persistent cell lineages, of which 17 were growing and dividing before the Amp exposure (Fig. 2A and Supplementary Video 8-10); the presence or absence of growth and division of 5 persistent cell lineages was indeterminate due to defocusing of cell images, crowding with neighboring cells, or translocation of cells within microchambers. Therefore, the dominance of non-dormant persisters in exponential phase was unchanged even in M9 medium.

Radical morphological changes of cell bodies were also observed in many non-dormant cells in M9 medium, including those in the persistent cell lineages. Surprisingly, some of the L-form-like cells crawled around like amoeba cells within the microchambers, detaching and leaving some parts of their cell bodies behind (Supplementary Video 11). Furthermore, rod-shaped regrowing cell populations emerged even from the small and left-behind cell bodies (Supplementary Video 11). These observations reveal the abilities of *E. coli* cells to sustain viability with abnormal morphologies and to restore rod shapes in the absence of agents that induced morphological changes.

Stationary phase environments increase the frequencies of dormant persisters

Several batch-culture assays have shown that stationary phase environments increase the frequencies of persister cells in bacterial cell populations [15, 16, 35]. We therefore sampled cells from early and late stationary phases in LB medium (Fig. S2A) and exposed them to 200 µg/mL of Amp in both batch and single-cell cultures.

As expected, the population killing curves showed significantly higher frequencies of surviving cells (Fig. 2B). The frequencies of surviving cells evaluated at the 3 h time point were 4.7×10^{-5} (2.9×10^{-5}-7.7×10^{-5}) for the cell populations sampled from the early stationary phase and 7.9×10^{-3} (4.8×10^{-3}-1.3×10^{-2}) for those from the late stationary phase (Fig. 2B).

Single-cell time-lapse measurements with the 40× objective detected 28 persistent cell lineages among 2.4×10^{5} drug-exposed cells in populations sampled from early stationary phase (Supplementary Video 12-14). Among them, we were able to determine growth states of 27 persistent cell lineages, of which 6 were non-dormant. However, the other 21 persistent cell lineages were dormant and exhibited no cell divisions before the Amp exposure (Fig. 2A). Therefore, the proportions of dormant persisters increased significantly in the cell populations sampled from early stationary phase.

For cell populations sampled from late stationary phase, we detected 69 persistent cell lineages among 6.6×10^{4} drug-exposed cells, finding that all but 3 indeterminate lineages were dormant before the Amp exposure (Fig. 2A and Supplementary Video 15-17). These results show that the predominance of different survival modes against Amp depends on the incubation duration under stationary phase conditions.

We found that many dormant cells sampled from late stationary phase remained intact under Amp exposure but did not regrow even after the drug removal. Most of these non-regrowing cells were plausibly viable as they were negative in propidium iodide (PI) staining (Fig. S5 and

Supplementary Video 18). Hence, it is plausible that these cells would eventually regrow as persisters with long lags. In fact, it has been shown by the single-cell measurements with a mother machine microfluidic device that the time to regrowth after drug removal is heterogeneous among dormant cells [23]. It should be noted that these late regrowers are detectable in the killing curve assay but not in the single-cell measurements with the MCMA microfluidic device due to the overgrowth of the early regrowers. Consequently, our single-cell measurements underestimate the frequency of persister cells in the population sampled from late stationary phase.

Stationary phase environments enhance survivability of dormant cells against Amp exposure.

To characterize the elongation and division dynamics of individual cells during the pre-culturing period in the MCMA device, we performed time-lapse experiments with cells sampled from early and late stationary phase using the 100× objective and observed lags in their regrowth (Fig. 3A-C, Supplementary Video 19 and 20). While most cells eventually restarted growth for populations sampled from early stationary phase, a significant fraction of cells remained non-growing and non-dividing during the pre-culture period of 2 h (Fig. 3B, C). The fractions of dormant cells in the cellular populations estimated by the elongation rates of individual cells immediately before the drug exposure were $(5.0\pm1.8)\times10^{-3}$ (n=1612), $(2.4\pm1.0)\times10^{-2}$ (n=251), and 0.26 ± 0.02 (n=818) in the cellular populations sampled from the exponential, early stationary, and late stationary phases, respectively (Fig. 3D-F). Therefore, the frequency of dormant cells in the populations increased significantly under stationary phase conditions.

We next asked whether the elevations of the fractions of persisters against Amp in the cellular populations sampled from the early and late stationary phases (Fig. 2B) were explainable by the increased fractions of dormant cells in the populations (Fig. 3). If the probability of

dormant cells becoming persisters (s_d) is independent of sampling growth phases and only dormant cells can survive, the frequency of surviving cells in the population (f_p) estimated from the population killing curves should follow

$$f_p = s_d P_d, \tag{1}$$

where P_d is the fraction of dormant cells in the population. Since all the surviving cells in populations sampled from late stationary phase were dormant persisters (Fig. 2A), we estimated s_d as $f_p^{(\mathrm{late})}/P_d^{(\mathrm{late})}$ = (3.0±1.6)×10^{-2} from the frequencies of surviving cells ($f_p^{(\mathrm{late})}$) and of dormant cells ($P_d^{(\mathrm{late})}$) in populations from late stationary phase. Then, we predicted the frequencies of persister cells from the frequencies of dormant cells (Fig. 3D and E) in the populations sampled from exponential and early stationary phases.

The results revealed that the observed frequencies of surviving cells in the populations were significantly smaller than the frequencies predicted by Eq. 1 (Fig. 3G). Note that the surviving cell frequencies under these conditions include the contributions of non-dormant persisters (Fig. 2A). Hence, f_p should be greater than the prediction of Eq. 1 if s_d were constant across the conditions. The result in Fig. 3G therefore indicates that the dormant cells in the population sampled from exponential and early stationary phases produced fewer surviving cells than expected from the frequencies of dormant cells. We conclude that long incubation under stationary phase conditions enhanced the survivability of dormant cells against the drug exposure.

Growth phase dependent correlations between RpoS expression and persister trait

We examined expression levels of RpoS in individual cells, finding that dormant cells in populations sampled from late stationary phase expressed RpoS at high levels at the onset of the Amp exposure (Fig. 4A-F). Furthermore, we detected RpoS-mCherry foci in many dormant cells

from late stationary phase (Fig. 4G and H). This observation suggests that many of the RpoS-mCherry proteins were encapsulated into protein aggregates within the cells. This finding is consistent with previous results reported by [22] that long incubations under stationary phase conditions deepen *dormancy depth* and that the presence of protein aggregates characterizes the cells with deep dormancy.

Since dormant cells express RpoS at high levels and all the persisters emerge from the dormant cell fraction, high RpoS expression is necessarily found as the trait of persisters in the populations sampled from late stationary phase. However, dormant cells in populations sampled from exponential and early stationary phase did not necessarily express RpoS at high levels (Fig. 4A-F), and persister cells emerged even from the non-dormant cell fraction (Fig. 2A). Therefore, high RpoS expression cannot be a predictor of persister cells under these conditions.

Furthermore, in the populations sampled from late stationary phase, we noted that RpoS expression levels in persistent dormant lineages tended to be lower than those of all dormant cells (Fig. 4F, red points). The mean fluorescence intensity of RpoS-mCherry of the persistent dormant cells was 533$\pm$80 a.u. (n=8) immediately before the Amp exposure, whereas that of all the dormant cells was 758$\pm$ 19 a.u. (n=213; p=0.034, Welch's t-test). Therefore, high RpoS expression is not necessarily advantageous for dormant cells in terms of becoming persisters that can restart proliferation after drug removal.

Actively growing cells produce persisters against ciprofloxacin in exponential phase cultures

Having observed that the persisters against Amp in cellular populations sampled from exponential phase were predominantly non-dormant cells, we next investigated persistence against another antibiotic drug, ciprofloxacin (CPFX). While Amp is a β-lactam antibiotic targeting cell walls, CPFX is a fluoroquinolone antibiotic targeting DNA gyrase. MF1 cells in exponen-

tial phase in M9 minimal medium exposed to 1 μg/mL CPFX (16×MIC, Fig. S1B) exhibited a biphasic killing curve, confirming the presence of persistence in this condition (Fig. S6). The frequency of persisters evaluated at the 3 h time point was 7.5×10^{-4} (4.5×10^{-4}-1.3×10^{-3}).

We conducted time-lapse experiments using the MCMA device (Fig. 5A, Supplementary Video 21, and Supplementary Video 22), and detected 148 persistent cell lineages that regrew after the exposure of 1 μg/mL CPFX for 6 h among 8.3×10^{5} drug-exposed cells. We found that cells grew and divided before the CPFX exposure in the detected persistent cell lineages (with 32 indeterminate lineages) (Fig. 5, Supplementary Video 21, and Supplementary Video 22). Unlike Amp, the CPFX exposure did not lyse cells but arrested their growth and division, including those in the persistent cell lineages. After the removal of CPFX, the persister cells resumed growth and became filamentous. The filamentous cells restarted cell divisions and produced normal-sized, and normally growing and dividing, progeny cells. The observed dynamics of the persistent cell lineages are consistent with what was reported for *E. coli* persisters against another fluoroquinolone antibiotic, ofloxacin [20]. These results confirmed that persisters against fluoroquinolone antibiotics targeting DNA gyrase in exponential phase were also non-dormant cells and thus persistence via non-dormant cells is not limited to Amp.

Discussion

Time-lapse single-cell observations with the MCMA microfluidic device enable direct visualization of persister cells existing at extremely low frequencies in isogenic bacterial cell populations. Contrary to the widely accepted view that pre-generated dormant cells are responsible for persistence, we found that actively growing cells produced persisters predominantly when the antibiotics were applied to the cellular populations sampled from exponential phases (Fig. 2A). Frequencies of dormant persisters increased in the cellular populations sampled from the early and late stationary phases (Fig. 2A). These results show that multiple survival modes are avail-

able for *E. coli* cells to achieve persistence even against the same drug. Furthermore, distinct survival modes coexisted within single persistent cell populations. In such cases, population-based analyses on bacterial persistence with an assumption of a single underlying mechanism would provide blurred results and bias our understanding of the phenomenon.

Interestingly, the predominant persisters against Amp in the cellular populations sampled from the exponential phases exhibited radical morphological changes and transitioned to the cell shapes that resemble L-form cells (Fig. 1D and E). L-form bacteria are deficient in cell walls but can sustain growth and division under osmoprotective conditions [31, 36]. L-form cells can be produced by treating bacteria with exogenous lytic enzymes or β-lactam antibiotics under osmoprotective conditions [36]. It is known that L-form bacteria are resistant to most antibiotics targeting cell wall synthesis, particularly β-lactams [31, 36]. Therefore, if the L-form-like cells produced by the Amp exposure could manage to protect themselves from osmotic pressure, they might be able to persist for an extended period under the Amp exposure. Since L-form cells are often found as antibiotic-resistant organisms and isolated from humans and animals in infectious diseases [36], this survival mode might be relevant to clinical settings. However, we also remark that such L-form-like cells did not appear upon CPFX exposure. Therefore, the transitions to L-form-like cells might be the general characteristics of non-dormant persisters against Amp and other β-lactam antibiotics, but these would not apply to the other non-β-lactam antibiotics.

The result that the incubation under stationary phase conditions enhanced the survivability of dormant cells against the Amp exposure (Fig. 3G) indicates that the states of dormant cells were not identical across the growth phases. In fact, many dormant cells in the populations sampled from the late stationary phase expressed RpoS at distinctly high levels in aggregated forms (Fig. 4F-H). It is important to note that many dormant cells sampled from the late stationary phase remained viable under the Amp exposure at least when the viability was judged by PI

staining (Fig. S5 and Supplementary Video 18). Since it is reported that the time to regrowth of dormant cells after drug removal is heterogeneous among dormant cells [23], it is plausible that these cells would eventually regrow after long lags. However, these late regrowers cannot significantly contribute to the regrowing cell populations due to the exponential penalties from the delay of regrowth.

It is also noteworthy that, in the cellular populations sampled from the late stationary phase, the RpoS expression levels of the dormant persisters that regrew after drug removal tended to be lower among the dormant cells (Fig. 4F). This observation may be consistent with a previous report that cells with shallow dormancy depth could restart proliferation quickly and become the main progenitors of the future population after drug removal [22].

As demonstrated here, our MCMA device can detect the persister cells existing at frequencies of 10^{-5} within a cellular population. This is the order at which one can detect persisters in most combinations of bacterial species and antibiotics, including clinically important ones [9, 12, 35]. Since multiple survival modes have been characterized in *E. coli* persistence, it would be crucial to unravel how individual cells of each bacterial species persist under various conditions of antibiotics exposure. Direct single-cell observations would unmask the diversity of persistence mechanisms and might enable rational designs of antibiotic treatments against bacterial infectious diseases.

Methods

E. coli strains and culture conditions

The main strain used in this study is *E. coli* strain MF1 (MG1655 *rpoS-mcherry*/pUA66-P_{rpsL}-*gfp*). pUA66-P_{rpsL}-*gfp* is a low-copy plasmid taken from the *E. coli* promoter library [27]. In the propidium iodide (PI) staining experiment, we used MG1655/pUA66-P_{rpsL}-*gfp* since the PI emission spectrum overlaps with that of mCherry. We also used the MG1655 strain as a control

in the MIC measurements.

The *mcherry* gene was amplified by PCR with the template pLmCherryK6Δterm and the primers rpoS-mcherry-F (CAAACGCAGG GGCTGAATAT CGAAGCGCTG TTCCGCGAGA GTGATTTTAT GGTGAGCAAG GGCGAGGA) and rpoS-mcherry-R (CAGCCTCGCT TGA-GACTGGC CTTTCTGACA GATGCTTACA TTCCGGGGAT CCGTCGACC) and integrated downstream of the *rpoS* locus on the chromosome of BW25113 strain by λ-Red recombination [37] to express the RpoS-mCherry fusion protein from the native locus. To construct the MF1 strain, the *rpoS-mcherry* gene and kanamycin-resistance gene flanked with two FRT sequences were transferred to MG1655 by P1 transduction. Kanamycin-resistance gene was removed by transforming pCP20 plasmid. The pCP20 plasmid was removed from the host cells by culturing them at 37°C overnight.

We cultured the cells with either Luria-Bertani (LB) broth (Difco) or M9 minimal medium (Difco) supplemented with 1/2 MEM amino acids solution (SIGMA) and 0.2% (w/v) glucose. All of the cultivation was conducted at 37°C.

Growth curve measurements

5 µL of the glycerol stock cell suspension was inoculated into 2 mL of LB or M9 minimal medium containing 40 µg/mL of kanamycin (Kan), and we cultured the cells at 37°C for 15 h (LB) or 16 h (M9) with shaking. Kan was added to the culture media to avoid the loss of the GFP-expressing plasmid (pUA66-P_{rpsL}-*gfp*) during the pre-culture. We diluted this pre-culture cell suspension with fresh LB or M9 medium (without Kan) to the cell density corresponding to the optical density at 600 nm (OD_{600}) being 0.005 (LB) or 0.01 (M9). The total volume of the diluted cell cultures was adjusted to 50 mL. After the dilution, we started culturing cells at 37°C with shaking. We sampled 100 µL of the cell cultures every one hour and measured OD_{600} with a spectrophotometer (UV-1800, Shimadzu). We repeated the measurements three times.

The mean and standard error of the logarithm of the OD_{600} were calculated for each sampling time point and plotted as the point and error bar in Fig. S2.

Killing curve assay

To measure killing curves in batch cultures, we first prepared 50 mL cell suspensions of OD_{600} = 0.005 (LB) or OD_{600} = 0.01 (M9) following the same protocol of growth curve measurements. We incubated the diluted cell suspensions at 37°C with shaking and sampled a portion of the cell cultures at a pre-determined time point (2.5 h for the exponential phase in LB; 8 h for the early stationary phase in LB; 24 h for the late stationary phase in LB; and 4 h for the exponential phase in M9). To match the pre-culturing conditions between the killing curve assays and the single-cell measurements, we diluted the extracted cell suspension with the fresh LB or M9 medium to the cell density with which the OD_{600} of the diluted cell suspension would reach 0.05 in the pre-culture of 2 h (LB) or 4 h (M9). The volume of the cell cultures was adjusted to 50 mL. After the pre-culture, we added the antibiotics (Amp or CPFX) to the cell culture and incubated it at 37°C with shaking. The concentrations of the antibiotics were adjusted to 200 μg/mL for Amp and 1 μg/mL for CPFX. We extracted 50 μL or 500 μL of the cell suspensions at the pre-determined time points to estimate the number of viable cells in the cellular populations.

To avoid the underestimation of viable cells from the non-culturability on solid agar [38,39], we estimated the viable cell number by a limiting dilution method. We conducted serial dilution of the extracted cell suspension (10× dilution in each dilution step) in 5 mL. We sampled 200 μL of each diluted cell suspension into a well in a 96-well plate. For each dilution condition, we dispensed the cell suspensions into 12 wells. We incubated the 96-well plates at 37°C for 36 h (LB) or 48 h (M9), and the turbidity of each well was inspected.

We found one or two dilution conditions for each sample taken from different time points where both turbid and non-turbid wells coexist among the 12 wells. Assuming Poissonian

allocation of viable cells, the proportion of non-turbid wells, x_0, is equal to e^{-dyN_v}, where N_v is the original concentration of viable cells, d is the dilution level, and y ($= 0.2$ mL) is the volume; then, $N_v = (yd)^{-1} \ln(1/x_0)$. Thus, we estimated the concentration of viable cells in the cell population as $N_v = (5/d) \ln(12/k)$ cells/mL, where k is the number of non-turbid wells. For example, if we found 3 non-turbid and 9 turbid wells for the cell suspension with the dilution of 10^{-6}, we could estimate the viable cell density as $N_v = 5 \times 10^6 \times \ln(12/3)$ cells/mL $= 7 \times 10^6$ cells/mL. When the coexistence of turbid and non-turbid wells was found in the two dilution conditions, we estimated the viable cell density of this time point by the geometric mean of the two estimated values.

We repeated the assay three times for each culture condition. The mean and standard error of the logarithm of the estimated viable cell density for each sampling time were calculated and shown as the point and error bar in Fig. 1A, 2B, S4, and S6.

MIC measurements

5 µL of the glycerol stock of the *E. coli* strain was inoculated into 2 mL of LB or M9 medium and incubated at 37°C with shaking for 15 h (LB) or 16 h (M9). We added Kan at the concentration of 40 µg/mL when we cultured the MF1 strain from the glycerol stock to avoid the loss of the GFP-expressing plasmid (pUA66-P_{rpsL}-*gfp*) during the pre-culture. The cell cultures were diluted with a fresh LB or M9 medium to the cell density corresponding to OD_{600} = 0.005 (LB) or OD_{600} = 0.01 (M9). The diluted cell cultures of 2 mL were incubated at 37°C with shaking for 2.5 h (LB) or 3 h (M9) to let the cell cultures enter exponential phases. The cell cultures were again diluted with a fresh medium to the cell density corresponding to OD_{600} = 0.0002. We mixed 100 µL of the diluted cell suspension with 100 µL of the medium containing Amp or CPFX and dispensed it into a well of the 96-well plate. We prepared 12 antibiotic concentration conditions with 2-fold serial differences (Amp: 2^{-2}-2^{8} µg/mL (+0 µg/mL); CPFX:

2^{-9}-2^{1} μg/mL (+0 μg/mL)). We used three wells for each drug concentration condition. The cell cultures in the 96-well plates were incubated at 37°C with shaking for 23 h. We measured the optical density at 595 nm (OD_{595}) of each well using a plate reader (FilterMax F5, Molecular Devices) and calculated the geometric mean of the three wells as the optical density of the cell culture in each drug concentration. We repeated the experiment three times and determined the MIC as the drug concentration above which the geometric mean of OD_{595} among the three replicate experiments were below 0.001.

Microfabrication

We fabricated microchamber arrays on glass coverslips by wet etching. The dimensions of each microchamber were 62 μm (w) × 47 μm (h) × 0.8 μm (d) for the array used in the experiments with a 100× objective (The number of microchambers in the array was 1240), and 53 μm (w) × 33 μm (h) × 0.8 μm (d) for the array used in the experiments with a 40× objective (The number of microchambers in the array was 22,302).

We first made the photomask for the microchamber array by laser drawing (DDB-201-TW, Neoark) on mask blanks (CBL4006Du-AZP, CLEAN SURFACE TECHNOLOGY). The photoresist on mask blanks was developed in NMD-3 (Tokyo Ohka Kogyo). The uncovered chromium (Cr)-layer was removed in MPM-E30 (DNP Fine Chemicals), and the remaining photoresist was removed by acetone. Lastly, the slide was rinsed in MilliQ water and air-dried.

For creating microchambers based on the pattern on the photomask, we first coated a 1,000-angstrom Cr-layer on a clean coverslip (NEO Micro glass, No. 1., 24 mm × 60 mm, Matsunami) by evaporative deposition and AZP1350 (AZ Electronic Materials) by spin-coating on the Cr-layer. After the pre-bake (95°C, 90 sec), we exposed the photoresist layer on the coverslip to UV light through the photomask using a mask aligner (MA-20, Mikasa). We developed the photoresist in NMD-3 and removed the Cr-layer uncovered by the photoresist in MPM-E30.

The coverslip was soaked in buffered hydrofluoric acid solution (110-BHF, Morita Kagaku Kogyo) for 14 minutes 20 seconds at 23°C for glass etching. The etching reaction was stopped by soaking the coverslip in milliQ water. The remaining photoresist and the Cr-layer were removed by acetone and MPM-E30, respectively.

We used a polydimethylsiloxane (PDMS) pad with bubble trap groove to control and change the culture conditions around the cells in the microchamber array. We follow the same procedure as that reported in [40] to fabricate the PDMS pad.

Chemical decoration of coverslip and cellulose membrane

To enclose the *E. coli* cells in the microchambers, we employed a method of attaching a cellulose membrane to a glass coverslip via biotin-streptavidin binding [28]. We chemically decorated glass coverslips with biotin and cellulose membranes with streptavidin. We followed the same protocol reported in [40] to prepare biotin-decorated coverslips and streptavidin-decorated cellulose membranes.

Preparation of conditioned media

As described below, we used the conditioned media to maintain the growth-suppressive conditions while preparing single-cell measurements of the cells sampled from the early and late stationary phases. We prepared 50 mL of the *E. coli* cell suspension at OD_{600} = 0.005 in the LB medium following the same procedure of growth curve measurements and incubated the cell cultures at 37°C with shaking. At the pre-determined time (8 h for the early stationary phase condition and 24 h for the late stationary phase condition), we spun down the cells at 2,200×g for 12 min. The supernatant was again spun down at 2,200×g for 12 min, and its supernatant was filtered with a 0.2-μm syringe filter. We used this filtered medium as the conditioned medium.

To prepare the agarose blocks of conditioned media, we dissolved 2% (w/v) low-melt agarose in the conditioned media with a microwave and solidified it in a plastic dish. To use this for attaching a cellulose membrane to a coverslip, we excised a piece of the conditioned medium pad with a sterilized blade and placed it on the cellulose membrane.

Sample preparation for time-lapse measurements

To prepare *E. coli* cells for the time-lapse single-cell observation, 5 μL of the glycerol stock of the MF1 cells was inoculated into 2 mL LB or M9 medium and incubated at 37°C with shaking for 15 h. The cell culture was diluted to OD_{600}=0.005 (in the case of LB medium), $OD_{600}=5\times10^{-6}$ (in the case of the 1000-fold more diluted condition in LB medium, Fig. 2A) or OD_{600}=0.01 (in the case of M9 medium) in a 50 mL fresh medium and again incubated at 37°C with shaking. We sampled cells from the cell culture at the pre-determined time points (2.5 h for the exponential phase in LB; 6 h for the exponential phase grown from the diluted cell suspension; 8 h for the early stationary phase in LB; 24 h for the late stationary phase in LB; and 4 h for the exponential phase in M9).

For the exponential phase samples (both LB and M9), 1 μL of cell suspension was sampled from the culture and placed on the microchamber array. We put a streptavidin-decorated cellulose membrane on the cell suspension and removed an excess suspension with a clean filter paper. A small piece of an LB or M9 agarose block (2% (w/v) agarose) was placed on the cellulose membrane and incubated at 37°C for 15 min to allow the membrane to adhere to the coverslip surface tightly. After removing the agarose block, a PDMS pad was attached to the coverslip via a Frame-Seal Incubation Chamber (9 mm×9 mm or 15 mm×15 mm, Bio-Rad). We connected the medium inlet and outlet of the PDMS pad to silicone tubes and started flowing an LB or M9 medium immediately at the flow rate of 2 mL/h using syringe pumps (NE-1000, New Era Pump Systems). We then registered the microchamber positions and started the

time-lapse measurements as described in the following section.

For the early and late stationary phase samples, we followed the same protocol except that we used the conditioned medium agarose pads made from the cell cultures of the corresponding growth phases to attach the cellulose membrane. We also flowed the liquid conditioned medium while registering the microchamber positions to maintain the growth-suppressive conditions. We switched the flowing media from the conditioned media to the fresh LB medium at the start of the time-lapse measurements to arrange the same duration of regrowth before the Amp exposure across the replicate experiments.

Time-lapse observation with the MCMA microfluidic device

We used Nikon Ti-E microscopes equipped with ORCA-flash camera (Hamamatsu Photonics) for the time-lapse observations. For the time-lapse observations with a 40× objective (Plan Apo λ, 40×/NA0.95), we acquired only bright-field images to monitor many microchamber positions simultaneously. For the time-lapse observations with a 100× objective (Plan Apo λ, 100×/NA1.45, oil immersion), we acquired bright-field, RpoS-mCherry fluorescence, and GFP fluorescence images. We used the LED (MCWHL2, Thorlabs) for fluorescence excitation. We maintained the temperature around the microscope stage at 37°C with a thermostat chamber (TIZHB, Tokai Hit).

The microscope was controlled from a PC using Micromanager [41]. The time-lapse intervals were 3 min in the measurements with the LB medium and 6 min in the measurements with the M9 medium.

In the time-lapse measurements of the cells in the LB medium, we first allowed the cells to grow in the microchambers flowing a fresh medium for either 1.5 h (the cells from the exponential phase) or 2 h (the cells from the early and late stationary phases). Then, we changed the flowing media to the one containing 200 μg/mL of Amp and observed the cells flowing

drug-containing medium for 3.5 h. We changed the flowing media again to the fresh medium containing no drug and allowed the viable cells to regrow.

In the time-lapse measurements of the cells in the M9 medium, we allowed the cells to grow in the microchambers for 4 h flowing a fresh M9 medium. We then switched the flowing media to the one containing 200 µg/mL Amp or 1 µg/mL CPFX and observed the cells under the drug-exposed conditions for 6 h. We again switched the flowing media back to the M9 medium containing no drug and allowed the viable cells to regrow.

Image analysis

We used a custom ImageJ macro to analyze the time-lapse images acquired with the 100× objective. This macro finds the outlines of the cells in each image and assigns the cell lineages based on the segmented cell image sequences. We corrected the errors in the segmentation and lineage assignments manually. The cell size (area), mean fluorescence intensity, and the connections in the cell lineages were exported into a text file for the data analysis.

We opened the images as a stack to find the persister cell lineages in the time-lapse images acquired with the 40× objective. From the end time point, we played back the stacked images to detect the microchambers with the surviving cells that stably regrew after the drug removal. We tracked back the persistent cell lineages and determined the existence of growth and cell divisions before the drug exposure.

To estimate the number of drug-exposed cells, we randomly selected 20 microchambers and counted the number of cells in each microchamber. We multiplied the averaged number of the cells in a microchamber by the number of the microchambers tracked in the time-lapse measurement. We used this number as the estimate of the total number of the drug-exposed cells in each experiment (Fig. 2).

Data analysis

Estimation of persister frequencies We estimated the persister cell frequencies from the population killing curves as the number of surviving cells at the time point of 3 h under the drug exposure relative to the initial number of cells at the onset of drug exposure. The error ranges of the persister cell frequencies were estimated by the error propagation of the standard errors of the numbers of cells at the two time points.

Estimation of killing rates from the killing curves We estimated the killing rates of the cell populations by fitting the population killing curves. We conducted non-linear fitting of double exponential (M9) or triple exponential decay (LB) curves to the logarithms of the experimental data using the Levenberg-Marquardt algorithm on Gnuplot. We used triple exponential decay curves to fit the killing curves in the LB medium because of the significant fitting deviations by the double exponential decay curves. In the main text, we reported the rates of the fastest and slowest decay terms as the killing rates of the initial and persistence phases, respectively. The standard errors of the decay rates estimated by fitting were reported as their error ranges.

Estimation of dormant cell fractions in cellular populations We analyzed the time-lapse data using a custom C script and exported the data for plotting the cell lineage trees. To determine the elongation rates of individual cells before the Amp exposure, we focused on the time window of 90 min immediately before the Amp exposure and calculated the averages of the instantaneous elongation rate $\frac{1}{\Delta t} \ln \frac{S(t+\Delta t)}{S(t)}$ over this time window, where $\Delta t = 3$ min is the time-lapse interval and $S(t)$ is the cell size (area) at time t. We did not include the time points of cell divisions for calculating the averages if cells divided in this time window. We regarded cell lineages with elongation rates below 0.013 min^{-1} as dormant and calculated the frequency of such lineages in each cell population sampled from a different growth phase.

Quantification of pre-exposure growth rate of cell lineages in exponential phase The pre-exposure growth rates of the cell lineages sampled from the exponential phase cultures were quantified by the mean division rates. For each single-cell lineage σ, the number of cell divisions before Amp exposure $D(\sigma)$ and the duration of pre-exposure period $T(\sigma)$ were obtained from the time-lapse images acquired with a 40$\times$ objective. The division rate of each cell lineage was estimated as $D(\sigma)/T(\sigma)$. The means and standard errors of division rate for the set of non-dormant persistent cell lineages (n=10) and for the set of non-surviving cell lineages (n=77) were reported in the main text. We extracted all the pre-exposure cell lineages for the non-dormant cell lineages, while we extracted 77 independent pre-exposure cell lineages originating from different individual cells at the start of the time-lapse observation by selecting either of sister cell lineages randomly at each cell division up to the onset of drug exposure.

Viability check by PI staining

We found that many dormant cells in the populations sampled from the late stationary phase remained intact during the Amp exposure but did not regrow after the drug removal. We examined the viability of the dormant cells flowing the media containing 1 μg/mL PI in the time-lapse measurements. In these experiments, we used the MG1655 pUA66-P_{rpsL}-*gfp* strain since the emission spectrum of RpoS-mCherry overlaps with that of PI. The preparation of the cells for the time-lapse measurements was the same as that used for the cells sampled from the late stationary phase, except that we flowed the media containing PI from the time point of adding Amp.

Materials availability

E. coli cell strains and vectors used in this study are available from the authors upon request.

References

[1] Levin, B. R. & Rozen, D. E. Non-inherited antibiotic resistance. *Nature Reviews Microbiology* **4**, 556–62 (2006).

[2] Dhar, N. & McKinney, J. D. Microbial phenotypic heterogeneity and antibiotic tolerance. *Current Opinion in Microbiology* **10**, 30–8 (2007).

[3] Lewis, K. Persister cells, dormancy and infectious disease. *Nature Reviews Microbiology* **5**, 48–56 (2007).

[4] Jayaraman, R. Bacterial persistence: some new insights into an old phenomenon. *Journal of Biosciences* **33**, 795–805 (2008).

[5] Balaban, N. Q. Persistence: mechanisms for triggering and enhancing phenotypic variability. *Current Opinion in Genetics & Development* **21**, 768–75 (2011).

[6] Maisonneuve, E. & Gerdes, K. Molecular mechanisms underlying bacterial persisters. *Cell* **157**, 539–548 (2014).

[7] Kester, J. C. & Fortune, S. M. Persisters and beyond: mechanisms of phenotypic drug resistance and drug tolerance in bacteria. *Critical Reviews in Biochemistry and Molecular Biology* **49**, 91–101 (2014).

[8] van den Bergh, B., Fauvart, M. & Michiels, J. Formation, physiology, ecology, evolution and clinical importance of bacterial persisters. *FEMS Microbiology Reviews* **41**, 219–251 (2017).

[9] Gomez, J. E. & McKinney, J. D. M. tuberculosis persistence, latency, and drug tolerance. *Tuberculosis* **84**, 29–44 (2004).

[10] Keren, I., Minami, S., Rubin, E. & Lewis, K. Characterization and Transcriptome Analysis of Mycobacterium tuberculosis Persisters. *mBio* **2**, e00100–11 (2011).

[11] Lechner, S., Lewis, K. & Bertram, R. Staphylococcus aureus persisters tolerant to bactericidal antibiotics. *Journal of Molecular Microbiology and Biotechnology* **22**, 235–44 (2012).

[12] Johnson, P. J. T. & Levin, B. R. Pharmacodynamics, Population Dynamics, and the Evolution of Persistence in Staphylococcus aureus. *PLoS Genet* **9**, e1003123 (2013).

[13] Liebens, V. *et al.* A putative de-N-acetylase of the PIG-L superfamily affects fluoroquinolone tolerance in Pseudomonas aeruginosa. *Pathogens and disease* **71**, 39–54 (2014).

[14] Bigger, J. W. Treatment of staphylococcal infections with penicillin by intermittent sterilisation. *The Lancet* **244**, 497–500 (1944).

[15] Balaban, N. Q. *et al.* Definitions and guidelines for research on antibiotic persistence. *Nature Reviews Microbiology* **17**, 441–448 (2019).

[16] Keren, I., Kaldalu, N., Spoering, A., Wang, Y. & Lewis, K. Persister cells and tolerance to antimicrobials. *FEMS Microbiology Letters* **230**, 13–18 (2004).

[17] Balaban, N. Q., Merrin, J., Chait, R., Kowalik, L. & Leibler, S. Bacterial persistence as a phenotypic switch. *Science* **305**, 1622–5 (2004).

[18] Svenningsen, M. S., Veress, A., Harms, A., Mitarai, N. & Semsey, S. Birth and resuscitation of (p)ppgpp induced antibiotic tolerant persister cells. *Scientific Reports* **9**, 1–13 (2019).

[19] Wakamoto, Y. *et al.* Dynamic persistence of antibiotic-stressed mycobacteria. *Science* **339**, 91–5 (2013).

[20] Goormaghtigh, F. & Melderen, L. V. Single-cell imaging and characterization of escherichia coli persister cells to ofloxacin in exponential cultures. *Science Advances* **5** (2019).

[21] Bamford, R. A. *et al.* Investigating the physiology of viable but non-culturable bacteria by microfluidics and time-lapse microscopy. *BMC Biology* **15**, 1–12 (2017).

[22] Pu, Y. *et al.* ATP-Dependent Dynamic Protein Aggregation Regulates Bacterial Dormancy Depth Critical for Antibiotic Tolerance. *Molecular Cell* **73**, 143–156.e4 (2019).

[23] Bakshi, S. *et al.* Tracking bacterial lineages in complex and dynamic environments with applications to growth control and persistence. *bioRxiv* 2020.03.27.006403 (2021).

[24] Orman, M. A. & Brynildsen, M. P. Dormancy is not necessary or sufficient for bacterial persistence. *Antimicrobial Agents and Chemotherapy* **57**, 3230–3239 (2013).

[25] Balaban, N. Q., Gerdes, K., Lewis, K. & McKinney, J. D. A problem of persistence: still more questions than answers? *Nature Reviews Microbiology* **11**, 587–91 (2013).

[26] Battesti, A., Majdalani, N. & Gottesman, S. The RpoS-mediated general stress response in Escherichia coli. *Ann. Rev. Microbiol.* **34**, 189–213 (2011).

[27] Zaslaver, A. *et al.* A comprehensive library of fluorescent transcriptional reporters for escherichia coli. *Nature methods* **3**, 623–8 (2006).

[28] Inoue, I., Wakamoto, Y., Moriguchi, H., Okano, K. & Yasuda, K. On-chip culture system for observation of isolated individual cells. *Lab on a Chip* **1**, 50–5 (2001).

[29] Umehara, S., Wakamoto, Y., Inoue, I. & Yasuda, K. On-chip single-cell microcultivation assay for monitoring environmental effects on isolated cells. *Biochemical and Biophysical Research Communications* **305** (2003).

[30] Shimaya, T., Okura, R., Wakamoto, Y. & Takeuchi, K. A. Scale invariance of cell size fluctuations in starving bacteria. *Communications Physics* **4**, 238 (2021).

[31] Errington, J., Mickiewicz, K., Kawai, Y. & Wu, L. J. L-form bacteria, chronic diseases and the origins of life. *Philosophical Transactions of the Royal Society B: Biological Sciences* **371** (2016).

[32] Jishage, M. & Ishihama, A. Regulation of RNA polymerase sigma subunit synthesis in Escherichia coli: intracellular levels of sigma 70 and sigma 38. *Journal of Bacteriology* **177**, 6832–5 (1995).

[33] Levin-Reisman, I. *et al.* Automated imaging with scanlag reveals previously undetectable bacterial growth phenotypes. *Nature Methods 2010 7:9* **7**, 737–739 (2010).

[34] Harms, A., Fino, C., Sørensen, M. A., Semsey, S. & Gerdes, K. Prophages and Growth Dynamics Confound Experimental Results with Antibiotic-Tolerant Persister Cells. *mBio* **8**, 1–18 (2017).

[35] Spoering, A. L. & Lewis, K. Biofilms and planktonic cells of pseudomonas aeruginosa have similar resistance to killing by antimicrobials. *Journal of Bacteriology* **183**, 6746–6751 (2001).

[36] Allan, E. J., Hoischen, C. & Gumpert, J. Bacterial l-forms. *Advances in Applied Microbiology* **68**, 1–39 (2009).

[37] Datsenko, K. A. & Wanner, B. L. One-step inactivation of chromosomal genes in escherichia coli k-12 using pcr products. *Proceedings of the National Academy of Sciences of the United States of America* **97**, 6640–5 (2000).

[38] Gelman, E., McKinney, J. D. & Dhar, N. Malachite green interferes with postantibiotic recovery of mycobacteria. *Antimicrobial Agents and Chemotherapy* **56**, 3610–3614 (2012).

[39] Nosho, K. *et al.* camp-crp acts as a key regulator for the viable but non-culturable state in escherichia coli. *Microbiology* 1–10 (2018).

[40] Yamauchi, S., Nozoe, T., Okura, R., Kussell, E. & Wakamoto, Y. A unified framework for measuring selection on cellular lineages and traits. *bioRxiv* (2021).

[41] Edelstein, A. D. *et al.* Advanced methods of microscope control using μmanager software. *Journal of Biological Methods* **1**, e11 (2014).

Acknowledgments

We acknowledge Nathalie Balaban for comments on the initial version of the manuscript and members of the Wakamoto lab for discussion. This work was supported by JST CREST Grant Number JPMJCR1927 (Y.W.); JST ERATO Grant Number JPMJER1902 (Y.W.); NIH Grant Number R01-GM097356 (E.K.); and Japan Society for the Promotion of Science KAKENHI Grant Number 17H06389 and 19H03216 (Y.W.).

Competing interests

The authors have declared that no competing interests exist.

Figure legends

Figure 1: **Detecting *E. coli* persistent cell lineages against Amp in exponential phase cultures.** **A**. Population killing curve. *E. coli* MF1 cells in exponential phase were exposed to 200 µg/mL of Amp, and the viable cell density in the cell cultures at each time point was determined by a limiting dilution assay (see Methods). The points and the error bars represent the means and the standard errors of the logarithm of the cell density among three replicate experiments. The dashed curve represents the fitting of the triple exponential decay curve to the data: $N(t) = 2.53 \times 10^7 \exp(-0.183t) + 2.84 \times 10^5 \exp(-5.73 \times 10^{-2}t) + 1.89 \times 10^2 \exp(-4.88 \times 10^{-3}t)$. The arrow indicates the duration of Amp exposure (3.5 h) in the time-lapse measurements. **B**. A micrograph of the microchamber array etched in a glass coverslip. **C**. Schematic drawing of cell cultivation in the MCMA device. Cells are enclosed in the microchambers by a cellulose membrane cover. A culture medium flows above the membrane. The medium in the microchambers is exchanged through diffusion across the membrane. Cells grow in a monolayer until they are thoroughly packed in the microchambers. **D**. Time-lapse images of the microchamber with a non-dormant persister cell. The right and middle image sequences show the RpoS-mCherry and GFP fluorescence images. The left image sequence shows the merged images of bright-field (grayscale), GFP (green), and RpoS-mCherry (red) channels. The red line to the left of the images indicates the images under Amp exposure. **E**. Enlarged micrographs of the cells in the non-dormant persistent cell lineage in D. **F**. Single-cell lineage tree that produced the non-dormant persister. The lineage tree which originated from the ancestor cell of the non-dormant persister cell is shown. The gray background indicates the period of the Amp exposure. The bifurcations of the branches represent cell divisions. The endpoints of the branches under the Amp exposure represent cell lysis events. **G**. Time-lapse images of the microchamber with a dormant persister cell. The correspondence of the image sequences to the acquisition channels is the same as in D. The white arrows indicate the dormant cell that eventually proliferated after the Amp exposure. **H**. Enlarged micrographs of the cells in the dormant persistent cell lineage in G. **I**. Single-cell lineage tree that produced the dormant persister.

Figure 2: **Growth-phase-dependent survival modes in the persistence against Amp. A**. Proportions of dormant and non-dormant persisters. Purple and green bars represent the frequencies of dormant and non-dormant persisters among the persistent cell lineages detected in the time-lapse measurements of the MF1 cells. Error bars represent binomial standard errors. The number of cells categorized into each survival mode is shown above the bar alongside the total number of persistent cells in each culture condition for which the presence or absence of growth and division was distinguishable. The table shows the estimated total numbers of the drug-exposed cells observed in the time-lapse measurements. **B**. Killing curves of cell populations sampled from different growth phases. 200 μg/mL of Amp was applied to *E. coli* MF1 cell populations sampled from exponential phase (magenta), early stationary phase (blue), and late stationary phase (yellow). Points and error bars represent means and standard errors of the logarithm of cell density among three replicate experiments. The data of the exponential phase is the same as those shown in Fig. 1A. The dashed curves represent the fitting of the triple exponential decay curves to the data: $N(t) = 1.50 \times 10^7 \exp(-0.236t) + 1.89 \times 10^5 \exp(-2.80 \times 10^{-2}t) + 2.22 \times 10^3 \exp(-8.29 \times 10^{-3}t)$ for the early stationary phase; $N(t) = 1.07 \times 10^7 \exp(-0.203t) + 5.41 \times 10^5 \exp(-2.65 \times 10^{-2}t) + 1.07 \times 10^5 \exp(-2.45 \times 10^{-3}t)$ for the late stationary phase.

Figure 3: **Stationary phase environments increase the frequency of dormant cells and enhance their survivability against Amp exposure. A-C**. Representative single-cell lineage trees of cells sampled from exponential (A), early stationary (B), and late stationary (C) phases. In these trees, cells were cultured under the flow of fresh LB medium containing no drug. The cells sampled from early and late stationary phases had been maintained under growth-suppressive conditions under the flow of conditioned media prior to t = 0 min (see Methods). **D-F**. Elongation rate distributions before Amp exposure. We quantified the elongation rates of individual cells during the time window of 30 min immediately before the Amp exposure. D, E, and F are the distributions for the cell populations sampled from exponential, early stationary, and late stationary phases, respectively. The vertical dashed lines represent the threshold value of elongation rate (0.013 min^{-1}) used to calculate the fractions of dormant cells shown in the plots. **G**. Relationship between the fractions of dormant cells (P_d) and the frequency of surviving cells against Amp exposure (f_p). The horizontal axis represents the fraction of dormant cells estimated in D-F. The vertical axis represents the frequency of surviving cells estimated from the frequencies of surviving cells in the population killing curves in Fig. 2B at the time point of 3 h after the Amp exposure. The error bars along the horizontal axis represent the binomial standard errors, and those along the vertical axis represent the standard errors of the frequencies of the surviving cells. The purple line represents $f_p = s_d P_d$ when s_d was assumed constant and estimated by the values of f_p and P_d for the late stationary phase condition. The gray background indicates the error ranges of s_d (1.5×10^{-2} - 4.6×10^{-2}). The dashed line represents the least-squares fitting of $f_p = e^{\alpha} P_d^n$ to the data in the log-log plot, and we found α = -2.4 $\pm$ 0.6 and n = 1.9 $\pm$ 0.2.

Figure 4: **Growth-phase-dependent expression levels of RpoS and its correlation with dormancy and persistence. A-C**. Distributions of RpoS-mCherry fluorescence intensity at the onset of Amp exposure. We evaluated the mean fluorescence intensity of RpoS-mCherry (i.e., a proxy for the intracellular concentration) in individual cells at the onset of the Amp exposure. The cells were cultured in the microchambers from exponential (A), early stationary (B), and late stationary (C) phases under the flow of fresh LB medium. The gray background indicates the intensity range in which the RpoS-mCherry fluorescence was indistinguishable from the background signals. **D-F**. Relationship between pre-exposure elongation rate and RpoS expression. The horizontal axis represents the elongation rates of individual cells immediately before the Amp exposure (see Fig. 3D-F for the distributions). The vertical axis represents the mean fluorescence intensity of individual cells at the onset of the Amp exposure. The vertical dashed lines represent the threshold elongation rate used to determine dormant cells. D, E, and F show the results for cells sampled from exponential, early stationary, and late stationary phases, respectively. The red points in F indicate cells that regrew after the Amp exposure of 3.5 h. **G**. A representative micrograph of the MF1 cells sampled from late stationary phase. The merged image of GFP and RpoS-mCherry fluorescence channels at the onset of the Amp exposure is shown. **H**. Enlarged micrographs of the dormant cells in the image of G. *a*, *b*, and *c* correspond to the respective squared frames in G. The cell in *a* regrew after the removal of Amp.

Figure 5: **Detecting *E. coli* persistent cell lineages against CPFX. A**. Time-lapse images of the microchamber that produced a persister against CPFX. The right and middle image sequences show the RpoS-mCherry and GFP fluorescence images. The left image sequence shows the merged images of GFP (green) and RpoS-mCherry (red) channels. The white arrows indicate the cells in the persistent cell lineage. **B**. Enlarged micrographs of the cells in the persistent cell lineage. **C**. Single-cell lineage tree that produced the persister cell. Unlike lineage trees under Amp exposure, the CPFX exposure did not lyse the cells. The black arrow indicates the persister cell lineage that regrew after the 6 h CPFX exposure.

Supplemental Figure legends

Figure S1: **MIC tests.** **A**. MIC test against Amp. The optical density at 595 nm of the *E. coli* cell cultures after the incubation of 23 h at 37°C in the LB media containing different concentrations of Amp (horizontal axis) is shown. Blue is for the MF1 strain, and magenta is for the MG1655 strain. The points (circles, squares, and crosses) represent the results of three replicate experiments. The dashed lines connect the geometric means of the replicates. The optical density values below 0.001 were plotted as 0.001 as they were indistinguishable from the fluctuation of background signals. **B**. MIC test against CPFX. The color correspondences to the *E. coli* strains are the same as that in A. The cells were incubated in the M9 media containing different concentrations of CPFX (horizontal axis) in this test. We measured the optical density at 595 nm after the incubation of 23 h at 37°C.

Figure S2: **Population growth curves of the MF1 strain.** **A**. The growth curve in the LB medium. The transitions of the optical density at 600 nm of the MF1 cell cultures are shown. The points represent the geometric means of three replicate experiments. The error bars represent the standard errors of the logarithm of the optical density, which are smaller than the point size. The vertical dashed lines represent the time points at which we sampled the cell cultures for the single-cell measurements and the killing curve assay. The magenta, blue, and yellow dashed lines indicate the sampling time points for the exponential, early stationary, and late stationary phases, respectively. **B**. The growth curve in the M9 medium. The points and the error bars (smaller than the point size) represent the same as those in A. The dashed line represents the time when cells were sampled for the single-cell measurements and killing curve assay.

Figure S3: **Experimental procedures for single-cell time-lapse measurements. A**. Loading *E. coli* cells in the MCMA device. A suspension of *E. coli* cells sampled from a batch culture is placed on the microchamber array etched in a coverslip. Placing a semi-permeable membrane on the cell suspension randomly seeds the cells in the microchambers. The semi-permeable membrane tightly seals the microchambers via the biotin-streptavidin binding. A PDMS pad attached to the coverslip via an adhesive frame seal chamber allows medium perfusion. The scale of the microchambers is exaggerated in this diagram for an intuitive explanation. **B**. Sequence of environmental conditions in the time-lapse measurements. *E. coli* cells were first grown under the flow of fresh medium. After that, we flowed a medium containing an antibiotic (Amp or CPFX) and allowed the surviving cells to regrow by exchanging the media back to the fresh medium.

Figure S4: **Comparison of the killing curves of the MF1 cells against Amp between LB and M9 media.** 200 µg/mL of Amp was exposed to the MF1 cell cultures in the exponential phases in LB (gray) and M9 (purple) media. The points represent the geometric means of the relative cell density to the values at the onset of the Amp exposure (0 min) among three replicate experiments. Error bars represent the standard errors of the logarithm of the relative cell density. The data for the LB medium are the same as those in Fig. 1A except that they are shown as the relative values in this plot. The purple dashed curve represents the fitting of the double exponential decay curve to the data for the cells in the M9 medium: $N(t) = (1 - 9.22 \times 10^{-5}) \exp(-7.47 \times 10^{-2} t) + 9.22 \times 10^{-5} \exp(-7.83 \times 10^{-3} t)$.

Figure S5: **Viability check of the non-regrowing dormant cells by PI staining.** The MG1655/pUA66-P_{rpsL}-*gfp* strain was used in this experiment. The cells sampled from the late stationary phase were observed in the MCMA microfluidic device with a 100× objective. PI was added to the flowing media from the time point for starting the Amp exposure. The right and middle image sequences show the images of the PI and GFP fluorescence, respectively. The left image sequence shows the merged images of the bright-field (grayscale), GFP (green), and PI (red) channels. The white arrows in the merged images at 330 min and 570 min indicate several dormant cells that did not regrow after the Amp exposure. We detected no fluorescence signals of PI in these cells, which suggests that they were viable.

Figure S6: **Population killing curve of the MF1 strain against CPFX.** MF1 cells in the exponential phase were exposed to the M9 medium containing 1 μg/mL of CPFX. The cell density at different time points was evaluated by a limiting dilution method (green). The points represent the geometric means of the relative cell density to the values at the onset of the Amp exposure (0 min) among three replicate experiments. The error bars represent the standard errors of the logarithm of the relative cell density. The green dashed curve represents the fitting of a double exponential decay curve to the data: $N(t) = (1-4.32\times10^{-3})\exp(-9.95\times10^{-2}t)+4.32\times10^{-3}\exp(-9.68\times10^{-3}t)$. The data points and the curve in purple are the results for the Amp exposure and the same as those of the "M9 Exponential phase" in Fig. S4.

Supplementary Video Legends

Supplementary Video 1. Time-lapse observation of the non-dormant persister of the MF1 strain against Amp. The time-lapse images were acquired with a 100× objective. Left: Merged images of the bright-field (grayscale), GFP (green), and RpoS-mCheerry (red) channels; Middle: GFP channel; Right: RpoS-mCherry channel. The medium conditions are indicated near the upper-left corner. The counter near the lower-right corner indicates the time in hour:min. Scale bar, 10 μm.

Supplementary Video 2. Time-lapse observation of the dormant persister of the MF1 strain against Amp. The time-lapse images were acquired with a 100× objective. Left: Merged images of the bright-field (grayscale), GFP (green), and RpoS-mCheerry (red) channels; Middle: GFP channel; Right: RpoS-mCherry channel. The medium conditions are indicated near the upper-left corner. The counter near the lower-right corner indicates the time in hour:min. Scale bar, 10 μm.

Supplementary Video 3. Simultaneous time-lapse observation of the drug responses of many individual cells using the MCMA microfluidic device. This movie shows a single field of view observed in a time-lapse measurement with the MCMA microfluidic device using a 40× objective. 40 microchambers can be visualized per position. We imaged 50-150 positions in a single time-lapse measurement. In this movie, one microchamber harbored a persistent cell lineage against Amp exposure (the third row from the top and the second column from the left). The medium conditions are indicated near the upper-left corner. The counter near the lower-left corner indicates the time in hour:min. Scale bar, 50 μm.

Supplementary Video 4. Time-lapse movie of the MF1 persisters against Amp in the LB medium (Exponential phase, Replicate experiment 1). This movie shows all the microchambers harboring persistent cell lineages in one of the replicated single-cell measurements of the MF1 cells against Amp cultured in the LB medium. The cells were sampled from the exponential phase. We used a 40× objective in this measurement. Scale bar, 10 μm.

Supplementary Video 5. Time-lapse movie of the MF1 persisters against Amp in the LB medium (Exponential phase, Replicate experiment 2). See the caption of Supplementary Video 4 for detail.

Supplementary Video 6. Time-lapse movie of the MF1 persisters against Amp in the LB medium (Exponential phase, Replicate experiment 3). See the caption of Supplementary Video 4 for detail.

Supplementary Video 7. Dormant persister that emerged in the cellular population sampled from exponential phase even after eliminating long-lagging bacteria. This movie shows a representative dormant cell lineage found in the population sampled from an exponential phase culture grown from a 1000-fold more diluted cell suspension.

Supplementary Video 8. Time-lapse movie of the MF1 persisters against Amp in the M9 medium (Exponential phase, Replicate experiment 1). This movie shows all the microchambers harboring persistent cell lineages in one of the replicated single-cell measurements of the MF1 cells against Amp cultured in the M9 medium. The cells were sampled from the exponential phase. We used a 40× objective in this measurement. Scale bar, 10 μm.

Supplementary Video 9. Time-lapse movie of the MF1 persisters against Amp in the M9 medium (Exponential phase, Replicate experiment 2). See the caption of Supplementary Video 8 for detail.

Supplementary Video 10. Time-lapse movie of the MF1 persisters against Amp in the M9 medium (Exponential phase, Replicate experiment 3). See the caption of Supplementary Video 8 for detail.

Supplementary Video 11. Amoeba-like locomotion of L-form-like *E. coli* cells in the microchambers. This movie shows representative three microchambers in which L-form-like *E. coli* cells exhibited amoeba-like locomotion. In this experiment, 200 μg/mL of Amp was exposed to the MF1 *E. coli* cells cultured in the M9 medium. Fission of cell bodies occurred in these cells during the locomotion. Furthermore, regrowing cell populations emerged from left-behind cell bodies.

Supplementary Video 12. Time-lapse movie of the MF1 persisters against Amp in the LB medium (Early stationary phase, Replicate experiment 1). This movie shows all the microchambers harboring persistent cell lineages in one of the replicated single-cell measurements of the MF1 cells against Amp cultured in the LB medium. The cells were sampled from the early stationary phase. We used a 40× objective in this measurement. Scale bar, 10 μm.

Supplementary Video 13. Time-lapse movie of the MF1 persisters against Amp in the LB medium (Early stationary phase, Replicate experiment 2). See the caption of Supplementary Video 12 for detail.

Supplementary Video 14. Time-lapse movie of the MF1 persisters against Amp in the LB medium (Early stationary phase, Replicate experiment 3). See the caption of Supplementary Video 12 for detail.

Supplementary Video 15. Time-lapse movie of the MF1 persisters against Amp in the LB medium (Late stationary phase, Replicate experiment 1). This movie shows all the microchambers harboring persistent cell lineages in one of the replicated single-cell measurements of the MF1 cells against Amp cultured in the LB medium. The cells were sampled from the late stationary phase. We used a 40× objective in this measurement. Scale bar, 10 μm.

Supplementary Video 16. Time-lapse movie of the MF1 persisters against Amp in the LB medium (Late stationary phase, Replicate experiment 2). See the caption of Supplementary Video 15 for detail.

Supplementary Video 17. Time-lapse movie of the MF1 persisters against Amp in the LB medium (Late stationary phase, Replicate experiment 3). See the caption of Supplementary Video 15 for detail.

Supplementary Video 18. Viability check of the non-regrowing dormant cells by PI staining. This movie shows the time-lapse observation of the MG1655/pUA66-P_{rpsL}-*gfp* cells sampled from the late stationary phase in the LB medium. We used a 100× objective in this measurement. Left: Merged images of the bright-field (grayscale), GFP (green), and PI (red) channels; Middle: GFP channel; Right: PI channel. PI was added to the flowing media from the start of the Amp exposure, as indicated by the medium conditions near the upper-left corner. We found many dormant cells that did not regrow even after the removal of Amp. They were visible in the GFP channel but negative with the PI staining. The counter near the upper-right

corner indicates the time in hour:min. Scale bar, 10 μm.

Supplementary Video 19. Time-lapse observation of the MF1 cells sampled from the early stationary phase. The time-lapse images were acquired with a 100× objective. The cells were sampled from the early stationary phase in the LB medium and monitored in the microchambers. 200 μg/mL of Amp was exposed to the cells from 2 h. The elongation rates and the RpoS-mCherry expression levels of individual cells before the Amp exposure were analyzed in Figs. 3 and 4. Left: Merged images of the bright-field (grayscale), GFP (green), and RpoS-mCheerry (red) channels; Middle: GFP channel; Right: RpoS-mCherry channel. The medium conditions are indicated near the upper-left corner. The counter near the lower-right corner indicates the time in hour:min. Scale bar, 10 μm.

Supplementary Video 20. Time-lapse observation of the MF1 cells sampled from the late stationary phase. The time-lapse images were acquired with a 100× objective. The cells were sampled from the late stationary phase in the LB medium and monitored in the microchambers. 200 μg/mL of Amp was exposed to the cells from 2 h. The elongation rates and the RpoS-mCherry expression levels of individual cells before the Amp exposure were analyzed in Figs. 3 and 4. Left: Merged images of the bright-field (grayscale), GFP (green), and RpoS-mCheerry (red) channels; Middle: GFP channel; Right: RpoS-mCherry channel. The medium conditions are indicated near the upper-left corner. The counter near the lower-right corner indicates the time in hour:min. Scale bar, 10 μm.

Supplementary Video 21. Time-lapse observation of the persister cells against CPFX (with 100× objective). The MF1 cells sampled from the exponential phase in the M9 medium were observed with the 100× objective. Left: Merged images of the GFP (green) and RpoS-mCherry (red) channels; Middle: GFP channel; Right: RpoS-mCherry channel. 1 μg/mL of CPFX was

exposed to the cells from 4 h. The medium conditions are indicated near the lower-left corner. The counter near the lower-right corner indicates the time in hour:min. Scale bar, 10 μm.

Supplementary Video 22. Time-lapse observation of the persister cells against CPFX (with 40× objective). This movie shows all the microchambers harboring persistent cell lineages in one of the replicated single-cell measurements of the MF1 cells against CPFX cultured in the LB medium. The cells were sampled from the exponential phase. We used a 40× objective in this measurement. Scale bar, 10 μm.

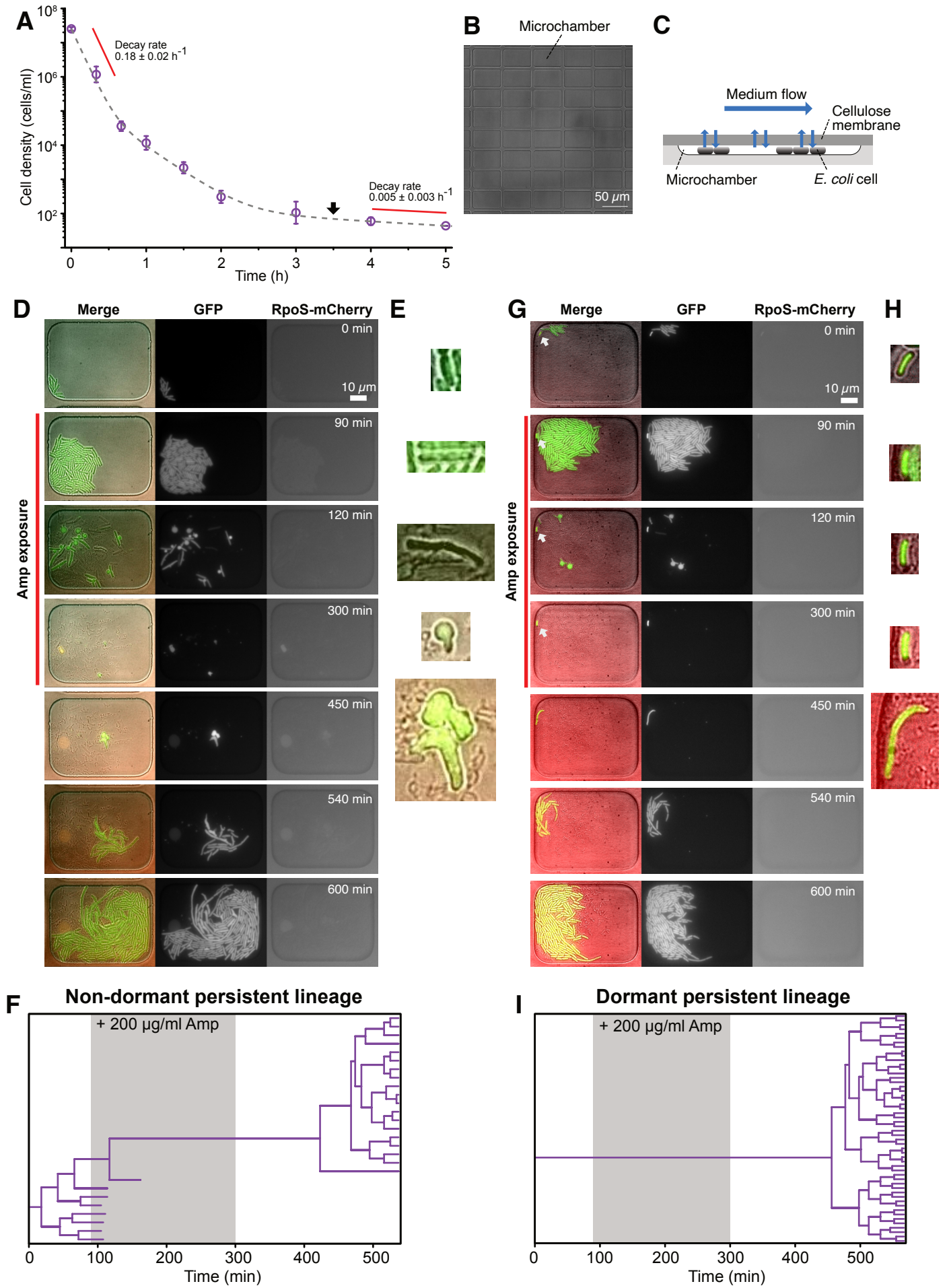

Figure 1. Umetani et al.

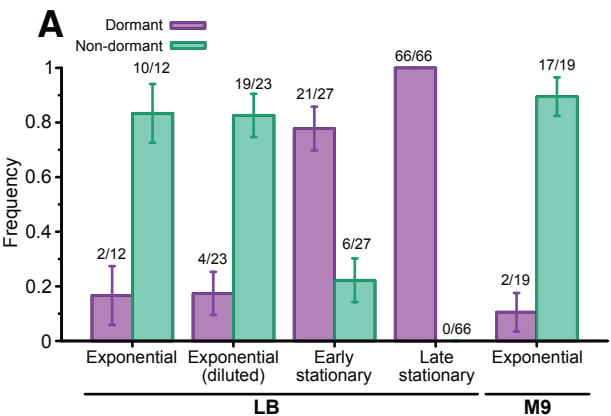

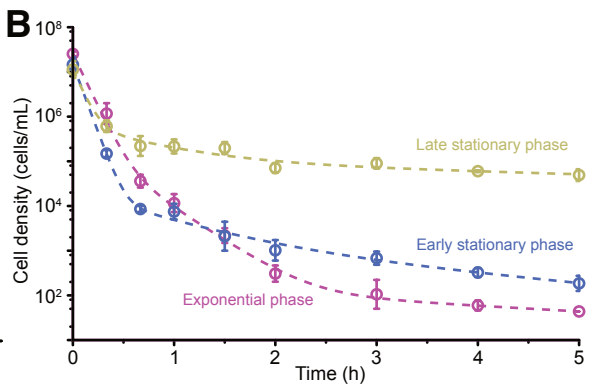

Medium	Sampling growth phase	Estimated total numbers of the drug-exposed cells observed (cells)
LB	Exponential	3.0×10^5
	Exponential (diluted)	9.9×10^5
	Early stationary	2.4×10^5
	Late stationary	6.6×10^4
M9	Exponential	1.1×10^6

Figure 2. Umetani et al.

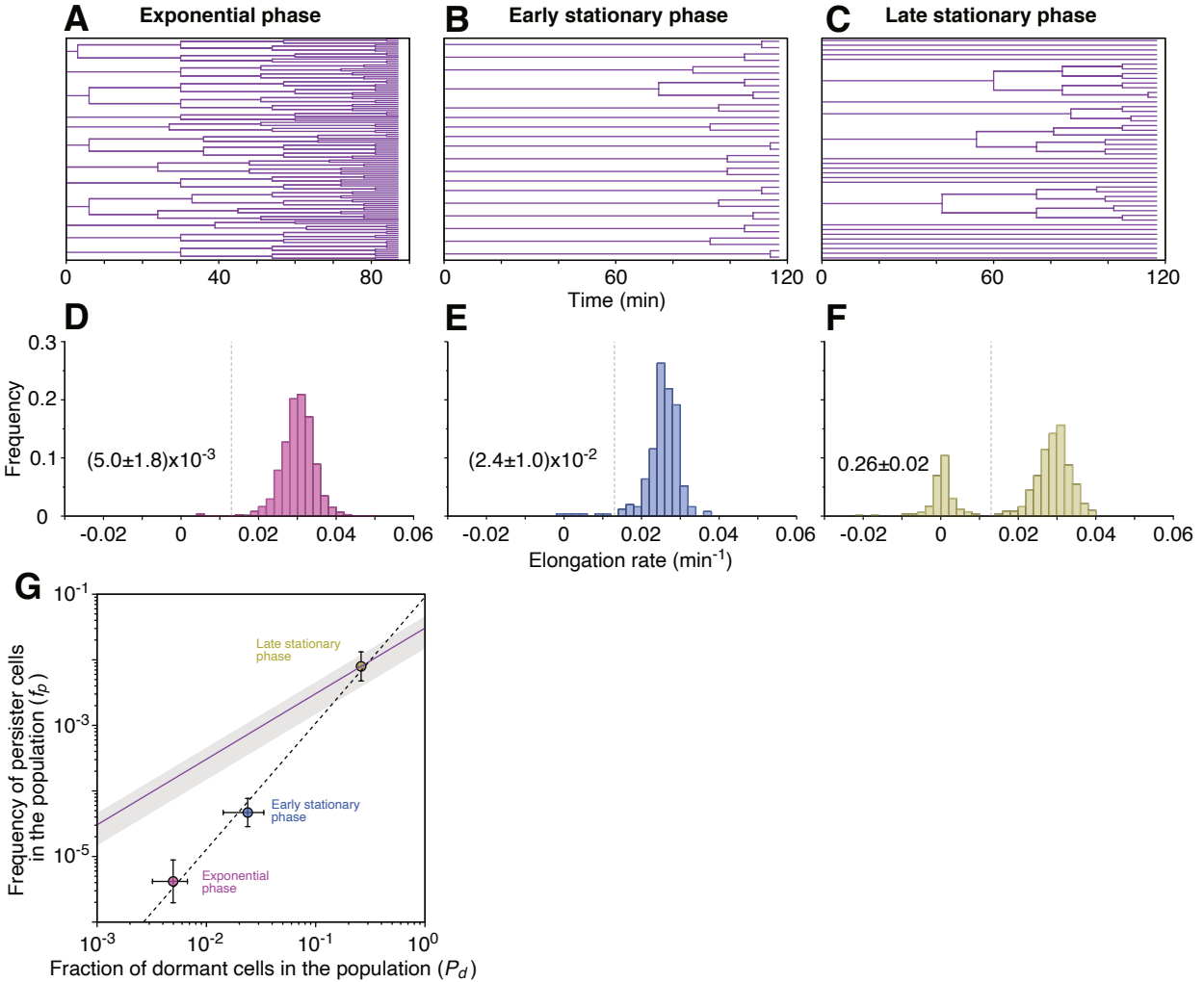

Figure 3. Umetani et al.

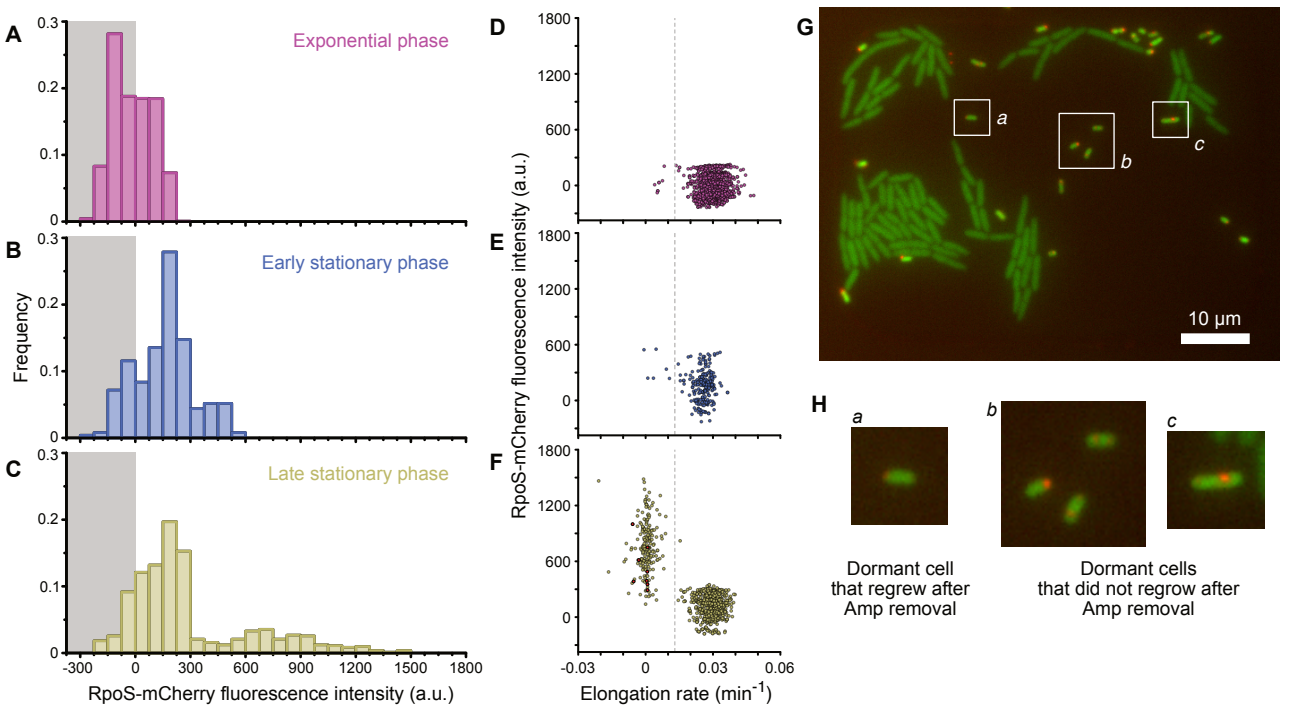

Figure 4. Umetani et al.

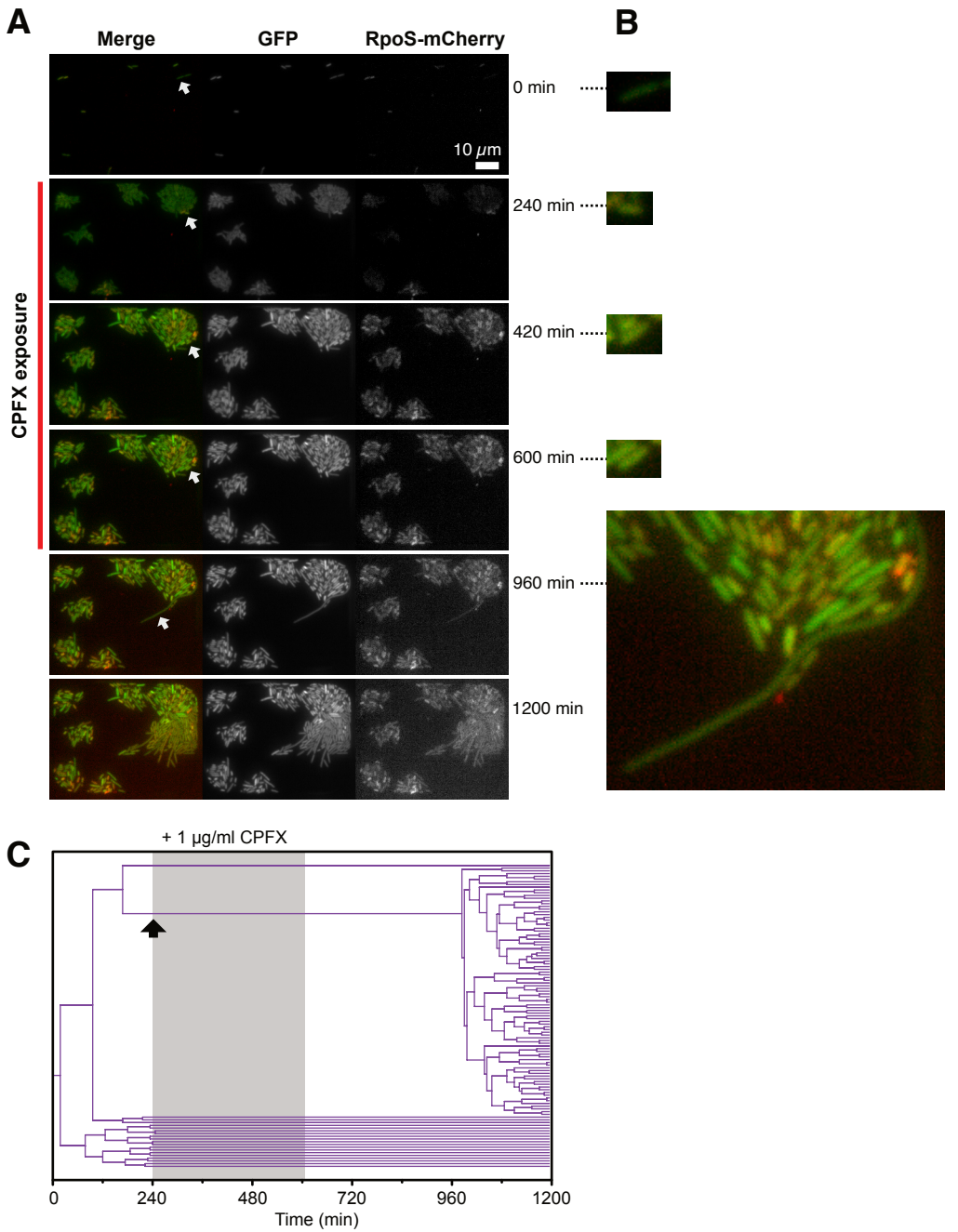

Figure 5. Umetani et al.

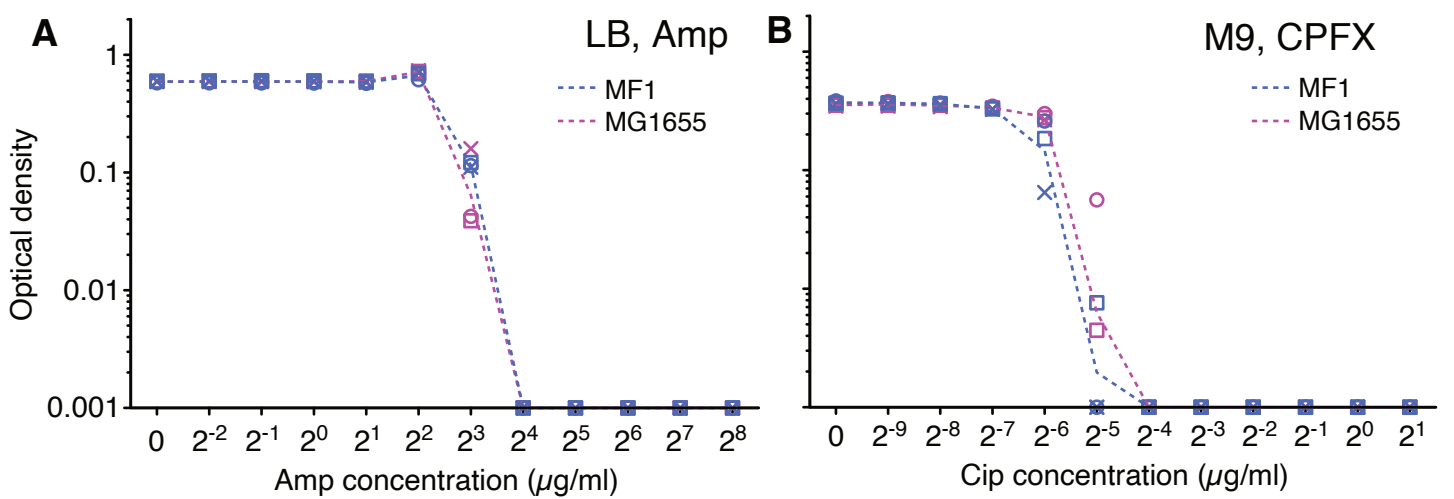

Fig S1. Umetani et al.

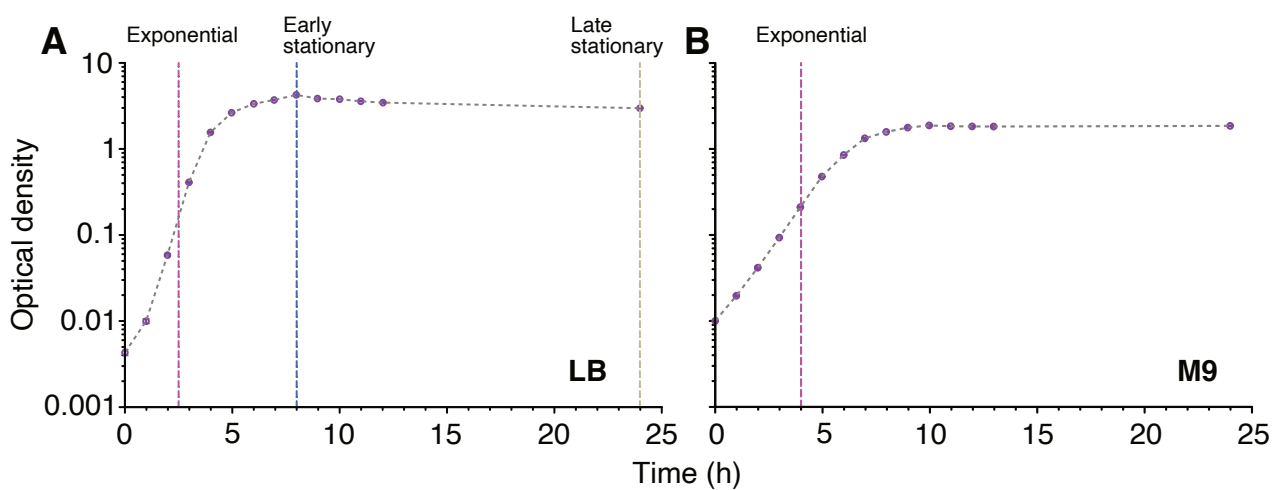

Fig S2. Umetani et al.

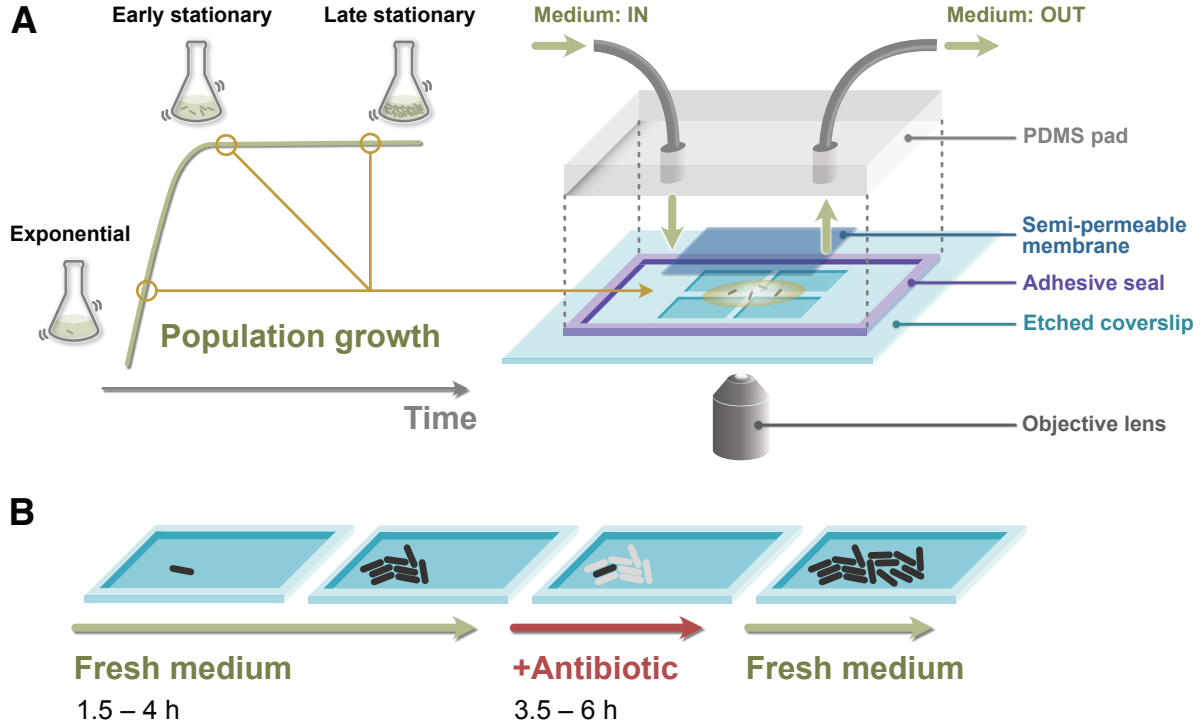

Fig S3. Umetani et al.

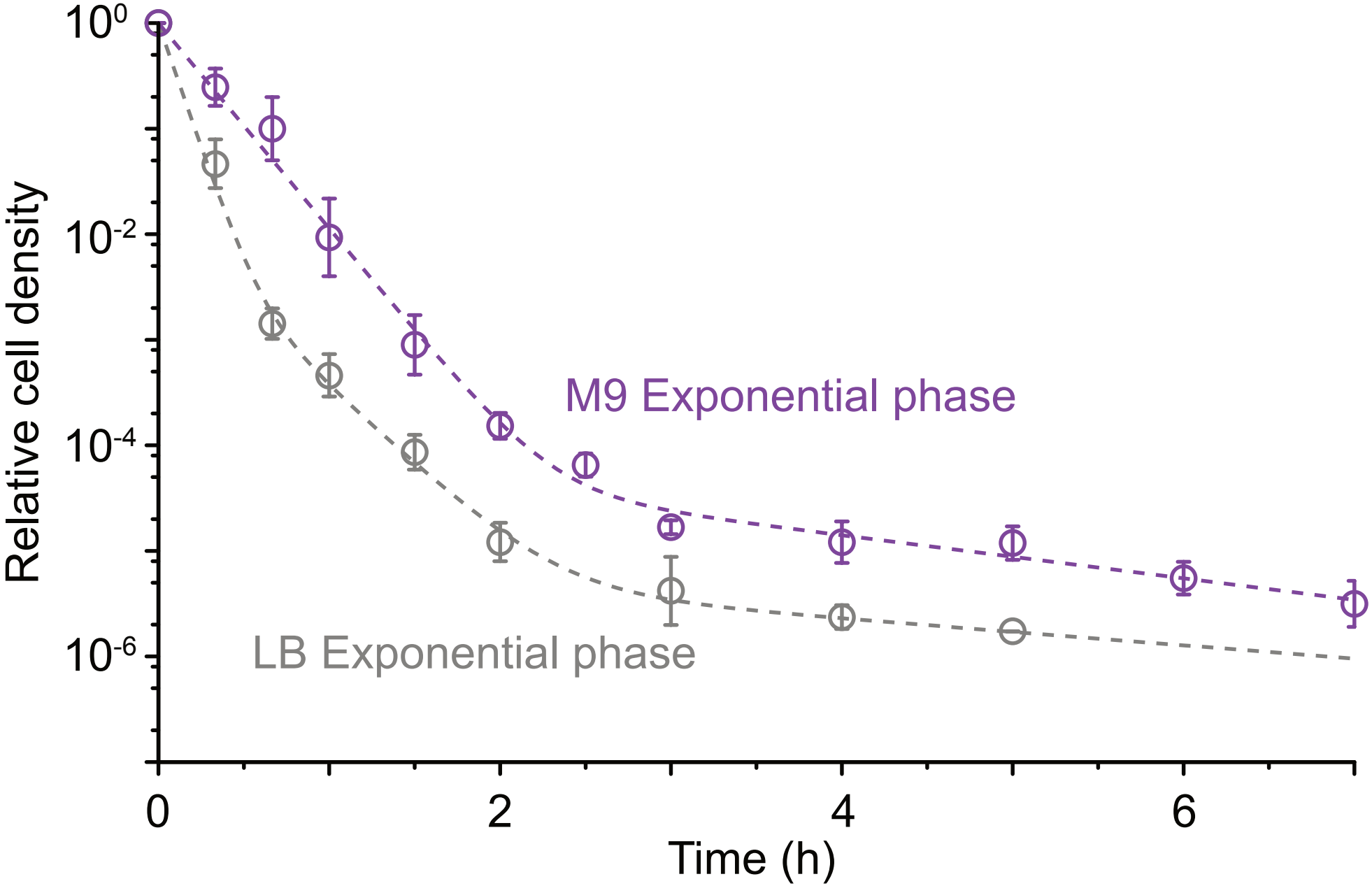

Fig S4. Umetani et al.

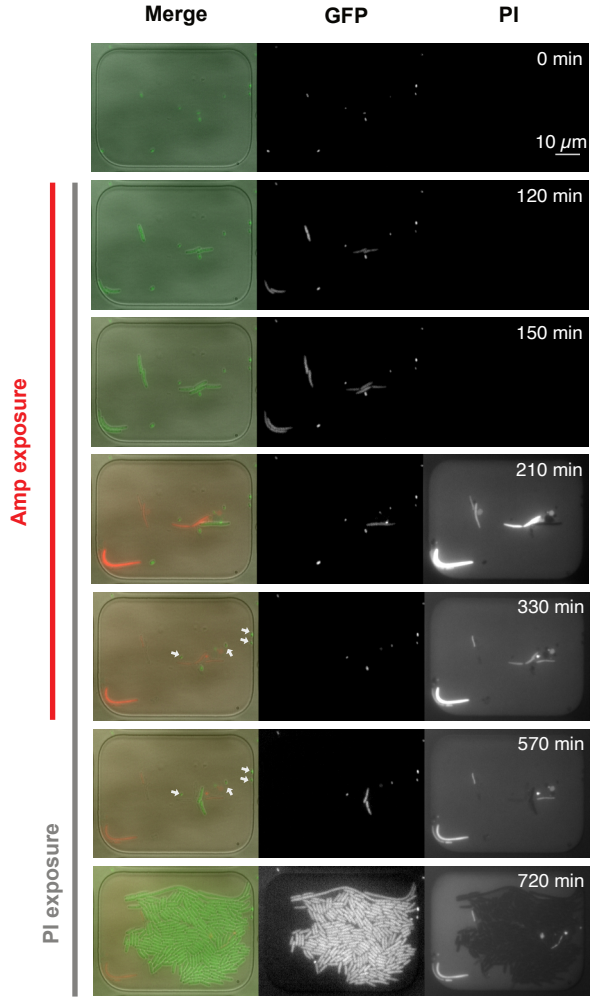

Fig S5. Umetani et al.

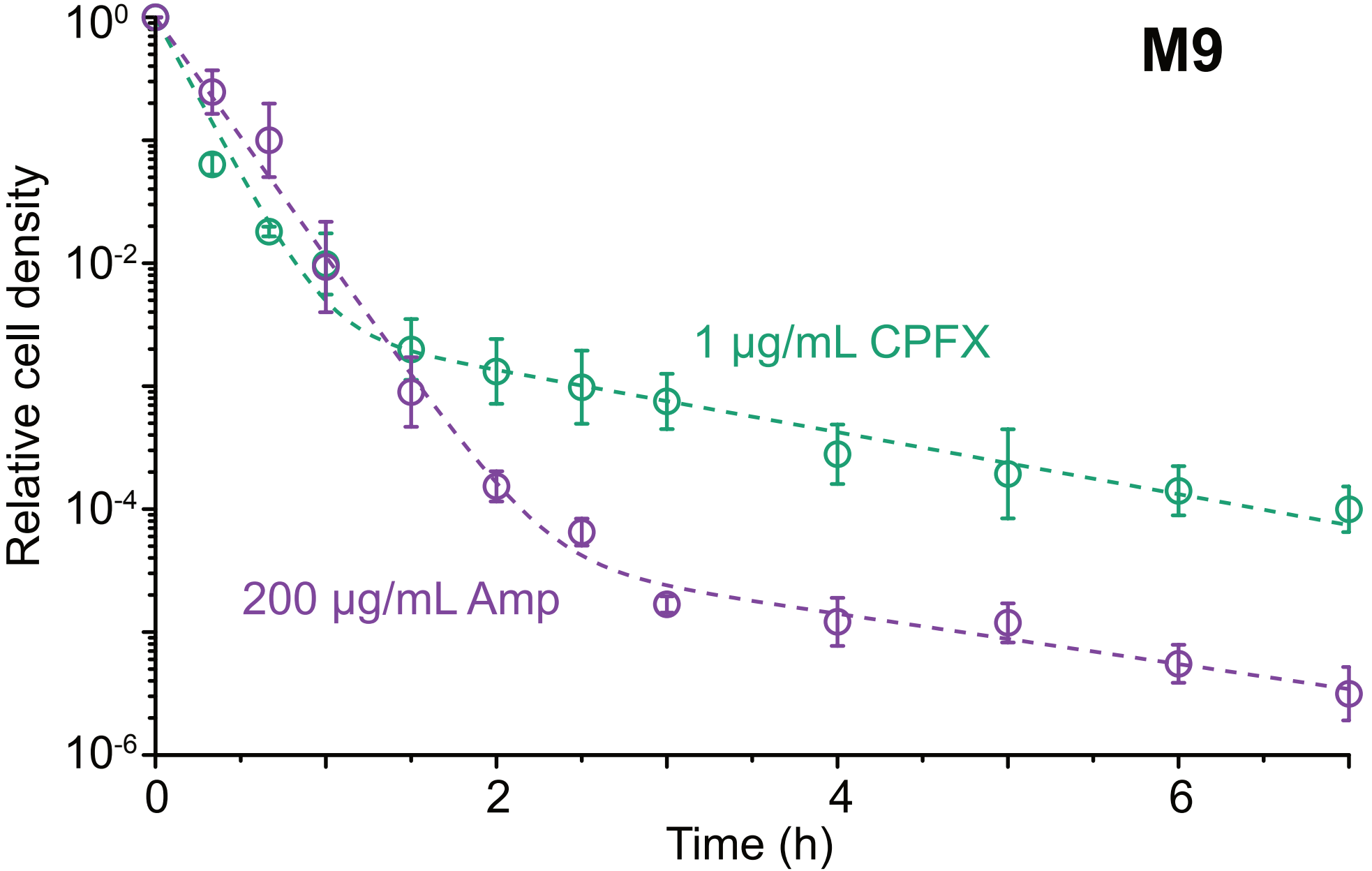

Fig S6. Umetani et al.